J. Micromech. Microeng. **19** (2009) 055007 (9pp) doi:10.1088/0960-1317/19/5/055007

Ultra-short pulsed laser PDMS thin-layer separation and micro-fabrication

Huan Huang and Zhixiong Guo[1]

Department of Mechanical and Aerospace Engineering, Rutgers, The State University of New Jersey, Piscataway, NJ 08854, USA

E-mail: guo@jove.rutgers.edu

Received 13 February 2009, in final form 16 March 2009
Published 15 April 2009
Online at stacks.iop.org/JMM/19/055007

Abstract

Thin-layer separation and micro-fabrication of poly(dimethylsiloxane) (PDMS) polymers are conducted via an ultra-short pulsed laser having a pulse width of 900 fs and lasing at an infrared wavelength of 1552 nm. The plasma-mediated ablation threshold of the PDMS is analyzed as 4.6 J cm^{-2} for single pulse irradiation. The threshold reduces with increasing pulses due to the accumulation effect, and the incubation factor is obtained as 0.52. The influences of two key factors—pulse overlap rate and irradiation pulse energy—on the ablation line width, internal ablation interface depth and ablation surface quality are scrutinized. To achieve quality separation and fabrication without visible thermal damage, a proper pulse overlap rate range of 1–2 pulses μm^{-1} is found with a modest irradiation pulse energy range of 1–1.5 μJ. Complete separation of thin PDMS layers of 20 μm thickness is realized. The separated thin layer is uniform, having a thickness fluctuation of ± 1 μm. A multi-width micro-channel interconnected network is fabricated, and the SEM images show that the ablation surface roughness is close to the depth of focus.

(Some figures in this article are in colour only in the electronic version)

1. Introduction

Poly(dimethylsiloxane) (PDMS) has been one of the most widely used silicon-based polymers for micro-electro-mechanical systems (MEMS), such as microfluidic systems [1–3]. The PDMS provides a highly interconnected crosslinked polymer structure which is accessible to nutrients and oxygen supply and has unique features such as controllability of mechanical properties and ability to not invoke an inflammatory or toxic response [4]. Its applications range from contact lenses and medical devices to elastomers [5].

Polymer micro-fabrication techniques include replica molding [6], stereolithography [7], electro-spinning [8], etc. Replica molding is of low cost, but requires multiple processing steps and has issues such as chemical biotoxicity to the polymers [6]; stereolithography can fabricate high aspect ratios and a wide variety of functional materials, but it builds up the structure slowly and allows only limited device volumes [7]; electro-spinning techniques can produce continuous nanofibers from various polymers, but require high voltage and a collecting substrate [8]. Recently, considerable efforts have been devoted to utilizing laser micro/nano-fabrication techniques [9, 10] because lasers can create complex microstructures resembling a natural tissue environment and have many advantages such as clean, non-invasive and precise processing. In addition, only an optical lens is needed to focus a laser beam on the microlevel for realization of microfabrication in laser direct writing techniques [11].

Ultra-short pulsed (USP) lasers with femtosecond or picosecond pulse duration have nowadays emerged as a promising tool in micromachining and processing [12–18] and biomedical applications [19, 20], owning to their unique interaction mechanisms with materials that are different from conventional lasers. When a short laser pulse is converged to a small focal spot, the energy flux at the focus is so high ($>10^{11}$ W cm^{-2}) that it induces optical breakdown, taking the material away via plasma-mediated ablation [12]. Substantial plasma generation and absorption enable the ablation of materials that are normally difficult to ablate by conventional

[1] Author to whom any correspondence should be addressed.

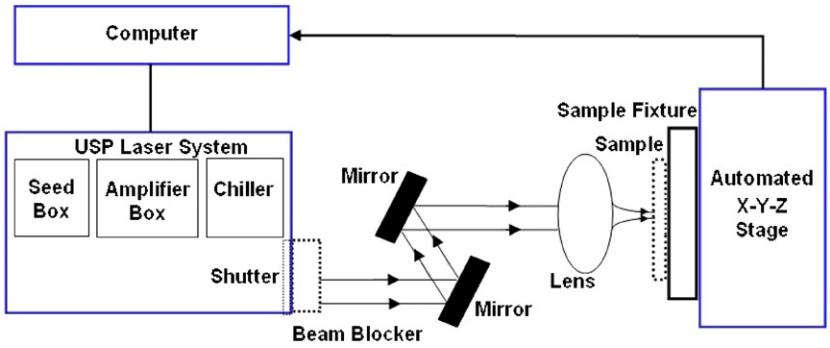

Figure 1. Sketch of the experimental setup.

lasers, such as transparent or low absorption materials [13, 14]. Another key benefit using USP lasers lies in their extremely short pulse duration such that interaction occurs before thermal diffusion ever takes place, leading to precise ablation with minimized thermal and collateral damage [15–18].

Although USP laser micromachining of tissues [15], polymers [16, 17] and glasses [18] has been extensively studied in recent years, studies on the laser thin-layer separation of dielectric materials such as the PDMS and tissues have not been reported in the literature. In the field of graft tissue implantation, tissues may have to be separated into layers, as a tissue in its entirety may not be necessary or appropriate for implantation. In the treatment of burn wounds, for instance, it may be necessary only to implant the epidermal layer of a skin allograft [21]. Unfortunately, there lacks effective means for separating thin layers of biological or artificial tissues. Furthermore, surgical treatment is frequently limited by the scarcity of adequate biological tissues available for reconstruction [22]. How to utilize a donor or artificial tissue as efficiently as possible is still a big challenge, because techniques using a mechanical cutter or surgical knife to separate a tissue into layers or cut the tissue into portions are often imprecise and can result in damage to the underlying layers and/or surrounding tissue [21]. Conventional pulsed laser ablation usually generates substantial heat during application, which can be transferred to the surrounding tissue and may result in melting or charring of tissues [23].

In this paper, the authors will investigate the separation and fabrication of PDMS thin layers and microstructures via the USP laser direct writing technique. First, the ablation threshold of the PDMS sample for single spot surface ablation via a USP laser operating at a wavelength of 1552 nm and having a pulse duration of 900 fs is determined. The incubation effect of multiple pulses is discussed. Then the surface line scanning ablation of the PDMS is featured. After that, the internal line and area ablations are inspected. Emphasis is placed on the examination of two key operation parameters—pulse energy and overlap rate. Finally, a multi-width microchannel network structure is fabricated and presented. This work yields useful information for the USP laser polymer and tissue microprocessing, artificial vasculature developing and development of microfluidic devices and systems.

2. Methods and materials

2.1. Experimental setup

The experimental setup is sketched in figure 1 and consists of four major systems: a commercial USP laser system, a beam delivery system, an automated work stage and a whole control system. The USP laser system is an erbium-doped fiber laser (Raydiance, Inc.) consisting of a seed box, an amplifier box and a chiller. Its lasing wavelength is centered at 1552 nm. The output pulses have a pulse width of 900 fs. The pulse repetition rate is tunable between 1 Hz and 500 kHz. The direct output pulse energy is adjustable between 1.0 and 5.0 μJ.

The beam delivery system is made up of a beam blocker, an astigmatism correction periscope (mirror) and an objective lens (Mitutoyo M Plan Apo NIR 20×, NA = 0.40, f = 20 mm). The measured focus spot size for the current laser system is about 8.0 μm. A digital power meter was used to measure the laser power loss in the beam delivery system and found that the total loss is 50%. Such a loss has been accounted for in the irradiation pulse energy values stated hereafter.

The work stage is composed of a lab-made fixture for holding the PDMS samples and a three-axis motorized high-speed high-precision translation stage (VP-25XA, Newport) for adjusting the laser beam focusing and for performing line and area scanning. The whole control system is a commercial RayOS^{TM} laptop interface for controlling the laser output parameters and for programming the motion pattern of the three-axis stage. All the experiments presented here were conducted in free space. During surface ablation processes, an evacuator system (FX225, EDSYN) which is not shown in figure 1 was also employed to collect plasma plume residue and debris.

2.2. Sample preparation

The PDMS samples were prepared by the Dow Corning Sylgard Elastomer 184 Kit. Proper amounts of the PDMS base and curing agent were taken by a weighing scale in a ratio of 10:1 and mixed well to a milky color consistency. The mixture was put into a vacuum chamber to evacuate the bubbles generated during mixing. The degassed PDMS assembly was placed on a hotplate at 65 °C for 4 h upon completion of the curing cycle. The refractive index of the PDMS is determined

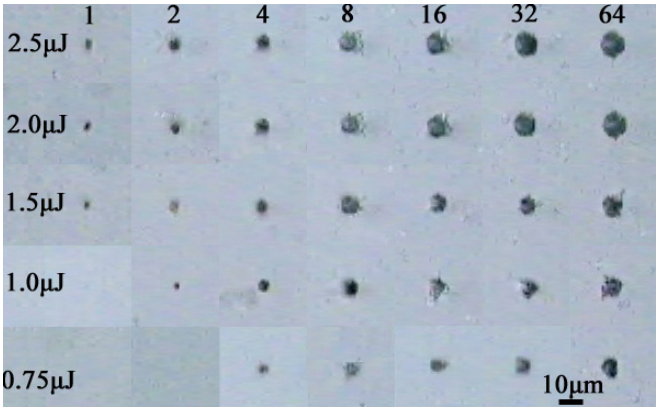

Figure 2. Microscopic view (400×) of an ablation craters array on the PDMS surface for single spot ablation.

by the curing time and temperature [24]. At a wavelength of 1552 nm, the current PDMS has a refractive index of 1.45. Measurement of the laser beam passing through the PDMS of 1 mm thickness gave a 15% attenuation loss.

2.3. Microscopy and measurement

The microtopography of the ablated PDMS lines, surfaces and channels was observed and characterized with an upright digital microscope (National Optical DC3-156-S) and a scanning electron microscope (SEM, AMRAY 1830I). A surface profiler (Dektak 3030) was also utilized to measure the thickness of the separated PDMS thin layers.

3. Results and discussion

3.1. Single spot and continuous line ablations

The ablation threshold of the PDMS samples via the current experimental setup should be first determined. Figure 2 shows the microscopic view of an ablated PDMS surface craters array. For each spot, the laser beam was normally focused onto a PDMS sample surface. The number in the array column represents the number of pulses deposited in a single spot with a pulse repetition rate of 1 Hz. The irradiation pulse energy (50% of the laser direct output) in the array rows varies from 0.75 to 2.5 μJ. Ablation damage is defined as any visible permanent modification to the surface observed by the microscope at 400× magnification. From figure 2, it is seen that a single pulse generates an ablation crater when the irradiation pulse energy is not less than 1.5 μJ. However, it needs two or four continuous pulses to generate a visible ablation crater when the irradiation pulse energy is 1.0 μJ or 0.75 μJ, respectively.

Figure 3 shows the measured ablation crater diameters for different irradiation pulse energies with different pulse numbers. It is found that the crater diameter enlarges as the pulse energy or pulse number increases.

For laser pulses with a Gaussian spatial beam profile, the maximum irradiation fluence F_0 can be calculated from the

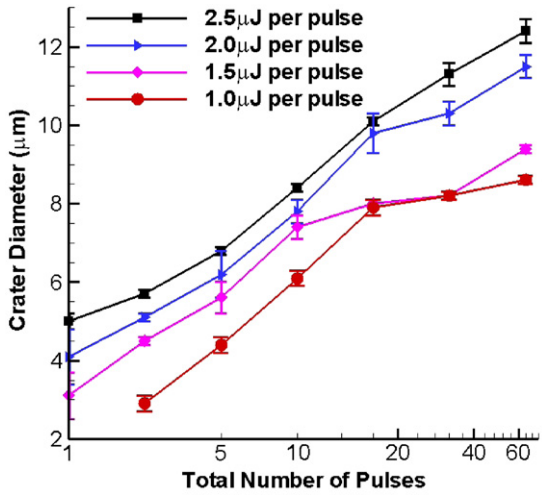

Figure 3. Effects of the pulse number and energy on the ablation crater diameter.

irradiation pulse energy E and the beam focus radius r as

$$F_0 = \frac{2E}{\pi r^2}. \tag{1}$$

If the maximum fluence (F_0) exceeds the ablation threshold fluence (F_{th}), then the squared diameter (D^2) of the ablation crater is correlated with F_0 by [25]

$$D^2 = 2r^2 \ln\left(\frac{F_0}{F_{\text{th}}}\right). \tag{2}$$

Therefore, it is possible to determine the Gaussian beam radius and the ablation threshold by plotting the diameter of the single pulse ablation crater versus the incident pulse energy. This technique is well described in [25], and is thus not repeated here. From the data in figure 3, the focal beam radius in the ablation spot is determined to be $r = 3.9$ μm and the ablation threshold of the PDMS with single pulse irradiation is calculated as $F_{\text{th}} = 4.6$ J cm^{-2} for the current laser and optical system. This calculated beam focus diameter value ($2r = 7.8$ μm) is close to the Raydiance specified value (8.0 μm). Rubahn *et al* [26] summarized the ablation thresholds of the PDMS for various nanosecond lasers and found that the ablation threshold of the PDMS increases with an increasing ablation wavelength from ultraviolet (UV) to near-infrared.

For ablation with multiple pulses, the effect of incubation attributed to increased absorption due to the accumulation of damage or defects from individual pulses tends to reduce the ablation threshold. A relationship between the multi-pulse ablation threshold $F_{\text{th}}(N)$ and the single-pulse ablation threshold $F_{\text{th}}(1)$ is given by the accumulation model [27]

$$F_{\text{th}}(N) = F_{\text{th}}(1)N^{\xi-1}, \tag{3}$$

where N is the number of irradiation pulses and the exponent ξ is the so-called incubation factor. This factor depends on both the material and the laser properties. Figure 4 shows the experimental data for $\ln(NF_{\text{th}}(N))$ versus $\ln(N)$ and a least-squares fitting line from which the slope yields an incubation factor $\xi = 0.52$ for the PDMS.

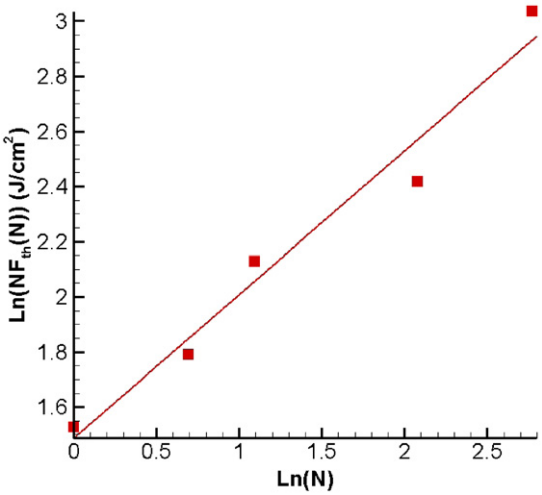

Figure 4. Multi-pulse incubation effect on the PDMS single spot ablation.

To enable practical thin-layer separation and micro-fabrication, the ablation features of line scanning must be understood because the continuity and quality of an ablation line depend on the overlap of many individual ablation craters. In the same time, the overlap intensity must be controlled in order to increase the working efficiency or to avoid any possible thermal damage due to over-deposition of energy. To this end, the pulse repetition rate and the moving speed of the work stage are two key factors. These two factors can be combined into one parameter—pulse overlap rate, which is the ratio of the pulse repetition rate to the stage moving speed and represents the pulse number per unit moving distance. Hence, it is needed to find a proper pulse overlap rate for PDMS thin-layer separation and micro-fabrication.

Figure 5 shows the single line scanning results at the PDMS surface with different pulse overlap rates and various pulse energies. Each line was scanned only once. In figure 5(*a*) where the pulse overlap rate is 0.2 pulse μm^{-1}, no continuous ablation line is observed. In the case with 1.0 μJ irradiation pulse energy, only about 30% of the line scanning area has been ablated. Even in the case with the maximum irradiation pulse energy (2.5 μJ), there is yet an unablated area in the scanning line. In figure 5(*b*), the pulse overlap rate increases to 0.5 pulse μm^{-1}; then only one ablation line with low irradiation pulse energy (1.0 μJ) is broken. By further increasing the pulse overlap rate to 2 and 10 pulses μm^{-1}, all the ablation lines are continuous as shown in figures 5(*c*) and (*d*), respectively. However, it is noted that the ablation lines

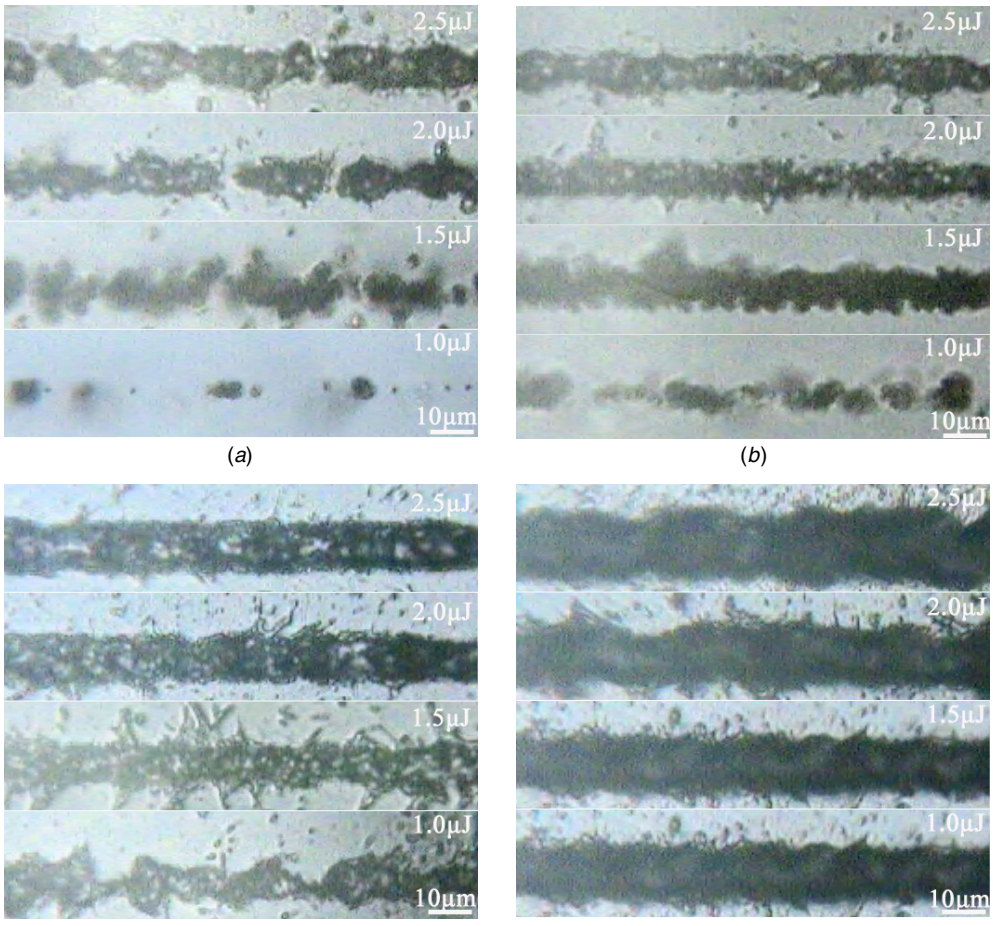

Figure 5. Microscopic view (1000×) of ablated single lines at the PDMS surface with different pulse overlap rates and various irradiation pulse energies. (*a*) 0.2 pulses μm^{-1}, (*b*) 0.5 pulses μm^{-1}, (*c*) 2 pulses μm^{-1} and (*d*) 10 pulses μm^{-1}.

Table 1. Test of laser parameters for the PDMS separation focusing 1 mm inside the PDMS.

Energy	0.75 μJ	1.0 μJ	1.5 μJ	2.0 μJ	2.5 μJ
Overlap rate					
0.2 pulse μm^{-1}	☆ □	☆ □	★ □	★ □	★ □
0.5 pulse μm^{-1}	☆ □	★ □	★ □	★ ■ ♦ ●	★ ■ ♦ ●
1 pulse μm^{-1}	☆ □	★ ■ ♦ ●	★ ■ ♦ ●	★ ■ ♦ ●	★ ■ ♦ ●
2 pulses μm^{-1}	★ □	★ ■ ♦ ●	★ ■ ♦ ●	★ ■ ♦ ●	★ ■ ◊ ●
5 pulses μm^{-1}	★ ■ ♦ ●	★ ■ ♦ ●	★ ■ ◊ ●	★ ■ ◊ ●	★ ■ ◊ ●
10 pulses μm^{-1}	★ ■ ♦ ●	★ ■ ◊ ●	★ ■ ◊ ●	★ ■ ◊ ●	★ ■ ◊ ●
50 pulses μm^{-1}	★ ■ ◊ ●	★ ■ ◊ ○	★ ■ ◊ ○	★ ■ ◊ ○	★ ■ ◊ ○

★: Ablation spark is observed.
☆: No ablation spark.
■: Can be separated into two layers.
□: Cannot be separated.
♦: Ablated surface looks normal.
◊: Ablated surface looks dark.
●: No obvious carbonized particle generated.
○: Obvious carbonized particle generated.

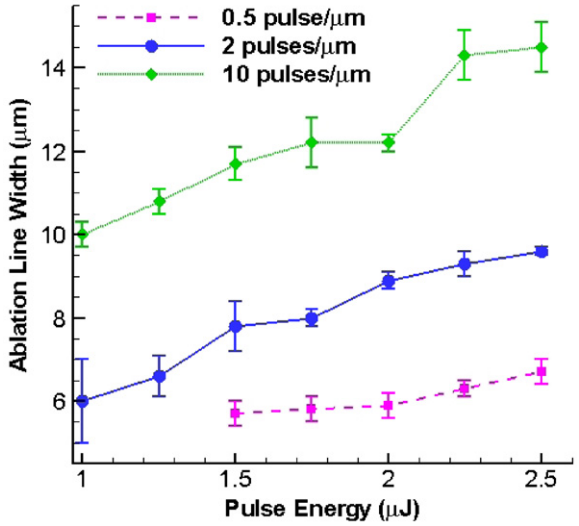

Figure 6. Plots of the single ablation line width versus the irradiation pulse energy.

in figure 5(*d*) are very dark, where thermal damage may be a concern.

Figure 6 plots the measured single ablation line width versus the irradiation pulse energy for three different pulse overlap rates. The line width uncertainty is due to two main factors: crater boundary and wavy motion (± 1 μm) of the translation stage. It is seen that the ablation line width increases as the irradiation pulse energy and overlap rate increase. The results in figures 5 and 6 show that 2 pulses μm^{-1} is a proper pulse overlap rate for line ablation.

3.2. Separation of the PDMS thin layers

For separation tests, three big PDMS samples were prepared. Each sample is cut into 35 small blocks, with a similar dimension of about 8 mm length, 2 mm width and 6 mm thickness. Each block was separation (internal area) scanned with the laser beam focused 1 mm below surface. The translation stage moved at a constant speed of 10 mm s^{-1} along the block length direction. The scanning lines are spaced 2 μm apart. For different blocks, the pulse repetition rate varied from 2 to 500 kHz, corresponding to a pulse overlap rate range between 0.2 and 50 pulses μm^{-1}. The surface irradiation pulse energy varied from 0.75 μJ to 2.5 μJ. Each test condition was repeated in three different sample blocks to minimize the impacts of performance fluctuation of the laser and the sample-to-sample variation.

Table 1 shows the test results for the separation of these blocks scanned with different sets of laser parameters. Comparisons are available with regard to the following aspects: (1) whether ablation sparks are observed during the laser scanning process, (2) whether the block can be separated by tweezers after the scanning, (3) whether the ablation surface looks normal or dark and (4) whether obvious carbonization at the separation surface is observed. From table 1, it seems that a wide range of the pulse overlap rate between 0.5 pulse μm^{-1} and 10 pulses μm^{-1} is fine for the PDMS separation. However, the selection of a proper pulse overlap rate must be in combination with the irradiation pulse energy. When the irradiation pulse energy is 0.75 μJ, for example, the pulse overlap rate should be in the range of 5–10 pulses μm^{-1}. When the irradiation energy is increased to 2.5 μJ, the pulse overlap rate should drop to the range of 0.5–1 pulse μm^{-1}. In terms of the fabrication efficiency, it is preferred to reduce the pulse overlap rate and thus apply high pulse energy.

Figure 7 visualizes the separation scanned PDMS blocks with different sets of the pulse repetition rate and irradiation pulse energy. The photos were taken immediately after the laser scanning, but before peeling off. Since the PDMS is transparent against visible light, what visualized in the photos is the view of the separation interface. It is observed that the separation surface becomes darker and darker when the repetition rate increases from 20 to 500 kHz (i.e. pulse overlap rate from 2 to 50 pulses μm^{-1}) or when the irradiation pulse energy increases from 1.0 to 2.5 μJ. In terms of the minimization of possible thermal damage, it is more appropriate to operate at low laser pulse energy with a modest pulse overlap rate.

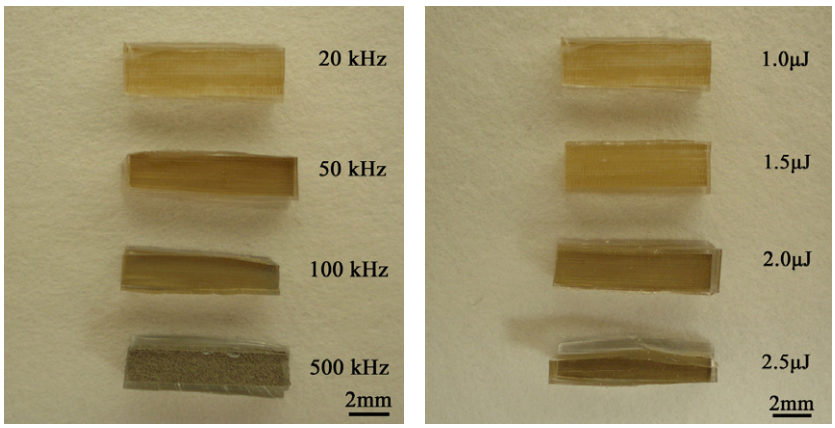

(*a*) (*b*)

Figure 7. Photos of the separation area scanned PDMS blocks: (*a*) with a constant irradiation pulse energy of 1.0 μJ and (*b*) with a constant pulse overlap rate 2 pulses μm^{-1}.

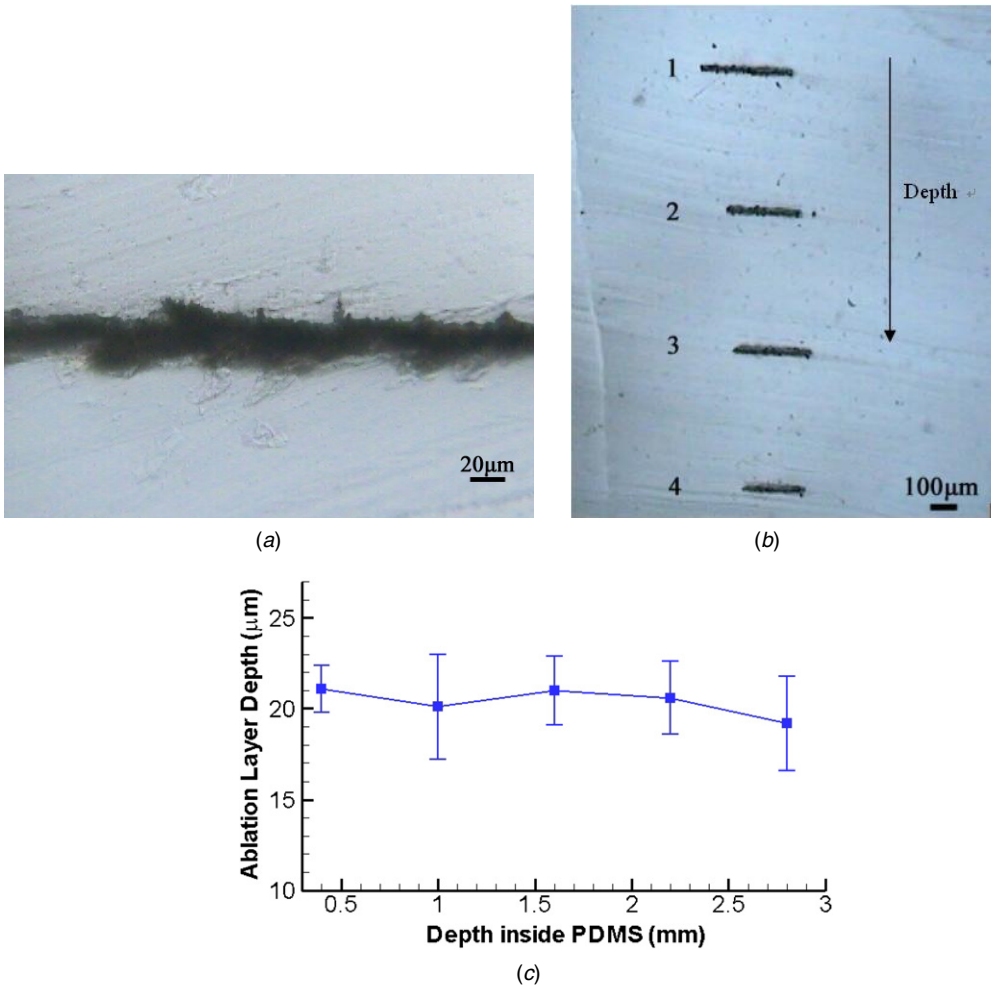

(*a*) (*b*) (*c*)

Figure 8. (*a*) Microscopic view (400×) of the ablation interface across the cross-section of a separation scanned PDMS block (1 mm deep, 1 pulse μm^{-1} and 1.0 μJ), (*b*) microscopic view (40×) of ablation cuts at different depths inside a PDMS sample (1 pulse μm^{-1} and 1.0 μJ) and (*c*) a plot of the measured ablation interface depth versus the laser beam focusing depth inside the PDMS (1 pulse μm^{-1} and 1.0 μJ).

Separation of the PDMS layers is based on the area scanning with the laser focusing on the target depth. Figure 8(*a*) visualizes the cutting interface of a PDMS block that was area scanned with the beam focusing 1 mm inside, pulse overlap rate at 1 pulse μm^{-1} and surface irradiation pulse energy at 1.0 μJ. The interface layer depth is measured to be about 20 ± 3 μm. This value is exactly twice the analyzed depth of the beam focus for this laser and lens system [28]:

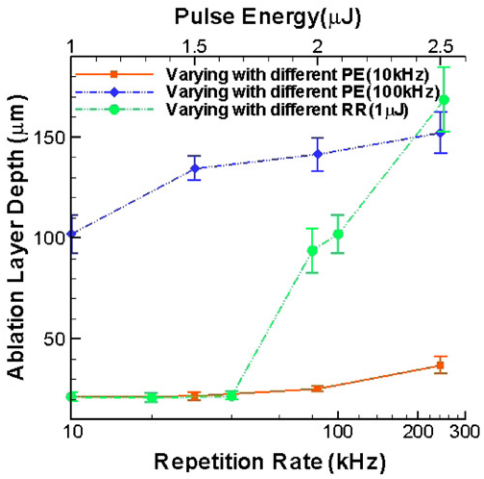

Figure 9. Effects of the pulse energy and repetition rate on the ablation layer depth with the beam focusing 1 mm beneath the PDMS surface (PE—pulse energy, RR—repetition rate).

$\Delta z = \pm 0.32\,\pi r^2/\lambda = \pm 10$ μm if we choose a typical spot size variation value of 5%.

Figure 8(*b*) shows the cutting interfaces at different layers inside one PDMS block with the laser beam focusing on different positions. The depth of the focus position under the PDMS surface is 1, 1.6, 2.2 and 2.8 mm, respectively, for the cutting interfaces from number 1 to number 4 as shown in figure 8(*b*). We actually generated another interface at a layer of 0.4 mm depth as well. It is not shown in figure 8(*b*) because of the view limit of the microscope used. Clear ablation occurred at all layers. The interface patterns for all layers are quite similar. Since the cuts at different layers were generated in the same block, it demonstrated the feasibility of performing three-dimensional micro-fabrication.

Figure 8(*c*) shows the ablation interface layer depths for different beam focusing positions from 0.4 to 2.8 mm inside the PDMS block. It is seen that the beam focusing position has slight effect on the ablation interface layer, because the beam focus spot size and depth are very weak functions of the beam length inside the PDMS [29] when the same objective lens is used. This also implies that the ablation threshold at any depth is a constant. It is worth mentioning that the laser intensity is attenuated with increasing depth because of light scattering and absorption in material. For the PDMS, it is optical transparent, and thus laser attenuation inside the PDMS is not a concern. We have also used the laser to separate real tissues, and the results will be reported soon.

Figure 9 displays the ablation layer depths with different pulse repetition rates and pulse energies at a constant stage moving speed of 10 mm s^{-1}. The beam was focused inside the block 1 mm beneath the surface. It is seen that both the pulse energy and the repetition rate influence the ablation interface layer depth. The effect of the pulse repetition rate is more pronounced when the repetition rate is over 40 kHz (i.e pulse overlap rate: 4 pulses μm^{-1}). The ablation layer depth increases substantially from about 20 to 170 μm as the pulse overlap rate increases from 4 to 25 pulses μm^{-1}.

Figure 10 demonstrates the PDMS layer separation after the laser scanning (2 pulses μm^{-1} and 1 μJ), where a thin layer is completely peeled off from a PDMS block via tweezers. There is no visible thermal and mechanical damage to the two separated layers. The thin layer thickness was measured by a surface profiler (DEKTAK 3030) and it is 20.3 μm thick on average. It has a very good uniformity with a fluctuation of ± 0.5 μm over the entire area.

The thickness of the separated thin layer is controllable by adjusting the position of the laser beam focal spot under the PDMS sample surface as shown in figure 8(*b*). The procedure consists of three steps: (1) the laser beam is aligned to be focused exactly on the PDMS sample surface via the observation of optimal spark generation on the surface, (2) the sample on the translation stage is moved toward the lens (z-direction) for a distance identical to the target thickness and (3) the sample is moved in the x–y plane to realize laser area scanning. Table 2 shows the measured thickness of different tests. For the three tests with a target thickness of 20 μm, the averaged thickness of the three samples is analyzed as 20.6 ± 1.7 μm. Thus, the fabrication is very precise.

3.3. Fabrication of the micro-channel network

Using the USP laser direct writing technique, a multi-width micro-channel network structure in the PDMS is fabricated and illuminated in figure 11. The red dye flow in the network shows that the fabricated channels are interconnected. The network is about 3.5 mm beneath the PDMS sample surface. The size of the channels varies from 50 to 400 μm. The laser parameters used in the fabrication were 2 pulses μm^{-1}

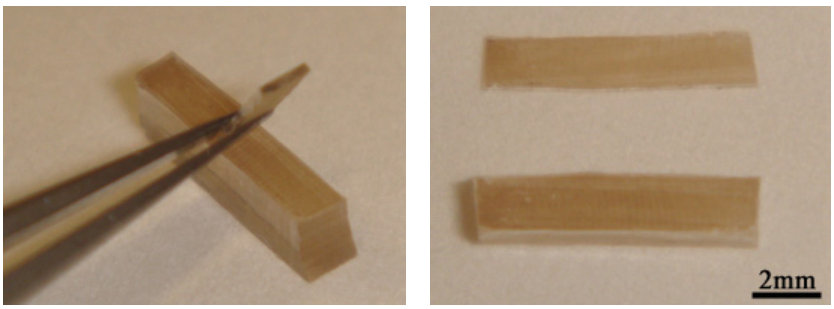

(*a*) peeling by tweezers. (*b*) the separated layers

Figure 10. Demonstration of the PDMS thin layer separation (2 pulses μm^{-1} and 1.0 μJ).

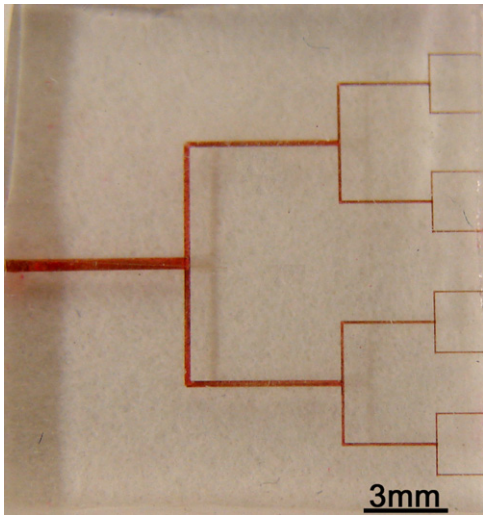

Figure 11. Photo of a multi-width micro-channel network with the red dye flow fabricated via the USP laser direct writing (2 pulses μm^{-1} and 1.0 μJ).

and 1.0 μJ. The line scanning space was 2 μm apart. The network structure could be significant for microfluidics [30]. It also shows the potential of the current fabrication technique in developing artificial vasculature in tissue engineering. Such structures would be difficult to achieve by using conventional fabrication methods. For example, undercuts cannot be directly done via the replication technology and use of a master is needed. However, the USP laser fabrication technique is simple and direct. It is also feasible to fabricate in three dimensions as demonstrated in figure 8(*b*).

The SEM images of the ablated network structure are exhibited in figures 12(*a*) and (*b*) for an ablated surface in the largest channel and a junction connecting two channels, respectively. From the images, the roughness of the ablated surface is estimated as 10 μm. Thus, the internal surface ablation roughness is close to the analytical value of the depth of focus. For taking the SEM image in figure 12(*b*), the network structure was cut into two halves so that the inside of the channel can be visualized with a tilted angle. It should be mentioned that the channel network results shown in figures 11 and 12 have not been treated with any other method such as etching which can smoothen the ablation surface.

Table 2. Thickness of the separated thin PDMS layers (dimension: 10 mm × 2 mm).

Sample no.	Measured thickness (μm)	Target thickness (μm)	Fluctuation (%)
1	18.7 ± 0.8	20	6.5
2	20.3 ± 0.5	20	1.5
3	22.8 ± 0.6	20	14
4	195.6 ± 5.5	200	2.2
5	212.5 ± 6.7	200	6.3
6	227.7 ± 9.3	200	14
7	330.2 ± 10.4	300	10
8	335.3 ± 5.5	300	12
9	315.8 ± 8.4	300	5.3

4. Summary

The ablation features of single spots and continuous lines at the PDMS via the USP laser direct writing are investigated. The ablation craters and lines are imaged for different irradiation pulse energies with various pulse numbers or pulse overlap rates. The fluence threshold for single spot ablation is determined to be 4.6 J cm^{-2}, and the incubation factor for multi-pulse ablation is found as 0.52. The ablation line width increases as the pulse energy or overlap rate increases. The pulse overlap rate is defined as the ratio of the pulse repetition rate to the scanning speed. This rate is found to be a key factor for both generating continuous and uniform line features and minimizing possible thermal damage. For PDMS thin-layer separation and micro-fabrication using the present instrument, the pulse overlap rate can be chosen in a wide range between 0.5 pulse μm^{-1} and 10 pulses μm^{-1}. However, a proper pulse overlap rate should accommodate the irradiation pulse energy. When the irradiation pulse energy is 0.75 μJ, an appropriate pulse overlap rate should be in the range of 5–10 pulses μm^{-1}; whereas when the irradiation energy increases to 2.5 μJ, the pulse overlap rate should drop to the range of 0.5–1 pulse μm^{-1}. The use of a lower pulse overlap rate will improve the fabrication efficiency and minimize possible thermal damage, but may require higher pulse energy. Overall, 1–2 pulses μm^{-1} and 1–1.5 μJ are proper parametric ranges.

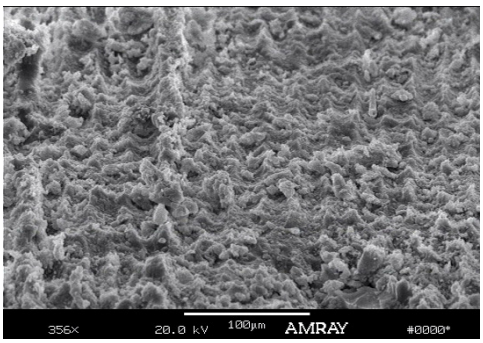

(*a*) an ablated channel surface.

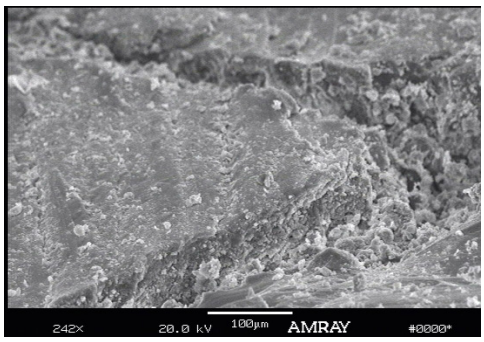

(*b*) a junction with titled angle.

Figure 12. SEM images of the multi-width micro-channel network structure.

Separation of the PDMS layers is based on the area scanning with the laser ablation inside. The separation of various PDMS thin layers and fabrication of a micro-channel network structure by the USP laser system are presented. The thickness of the separated thin layer is controllable via adjusting the laser focus spot position. For the three tests with a target thickness of 20 μm, the averaged thickness of the separated thin layers is 20.6 $\pm$ 1.7 μm. The fabrication is very precise. Both the pulse energy and the overlap rate influence the ablation interface layer depth. The effect of the pulse overlap rate is more pronounced when the overlap rate goes above the value of 4 pulses μm^{-1}. Below this value, the ablation layer depth is about 20 μm for 1–1.5 μJ pulse energy, twice the depth of focus. The fabricated network is shown to be interconnected. The roughness of the internal ablation surfaces in the network is close to the depth of focus.

Acknowledgments

This work was supported by the Musculoskeletal Transplant Foundation (MTF). The authors would like to thank Raydiance, Inc. for providing technical support.

References

[1] Jo B-H, Van Lergerghe L M, Motsegood K M and Beebe D J 2000 Three-dimensional micro-channel fabrication in polydimethylsiloxane (PDMS) elastomer *J. Microelectromech. Syst.* **9** 76–81

[2] McDonald J C and Whitesides G M 2002 Poly (dimethylsiloxane) as a material for fabricating microfluidic devices *Acc. Chem. Res.* **35** 491–9

[3] McDonald J C, Duffy D C, Anderson J R, Chiu D T, Wu H, Schueller O J A and Whitesides G M 2000 Fabrication of microfluidic systems in poly (dimethylsiloxane) *Electrophoresis* **21** 27–40

[4] Lotters J C, Olthuis W, Veltink P H and Bergveld P 1997 The mechanical properties of the rubber elastic polymer polydimethylsiloxane for sensor applications *J. Micromech. Microeng.* **7** 145–7

[5] DeBusschere B D, Borkholder D A and Kovacs G T A 1998 Design of an integrated silicon-PDMS cell cartridge *Proc. Solid-State Sensor Actuators Workshop (Hilton Head, SC)* pp 358–62

[6] Becker H and Gartner C 2000 Polymer microfabrication methods for microfluidic analytical applications *Electrophoresis* **21** 12–26

[7] Zhang X, Jiang X N and Sun C 1999 Micro-stereolithography of polymeric and ceramic microstructures *Sensors Actuators* **77** 149–56

[8] Yoshimoto H, Shin Y M, Terai H and Vacati J P 2003 A biodegradable nanofiber scaffold by electrospinning and its potential for bone tissue engineering *Biomaterials* **24** 2077–82

[9] Kancharla V V and Chen S 2002 Fabrication of biodegradable polymeric micro-devices using laser micromachining *Biomed. Microdevices* **4** 105–9

[10] Bityurin N 2005 Studies on laser ablation of polymers *Annu. Rep. Prog. Chem.* C **101** 216–47

[11] Lippert T 2004 Laser application of polymers *Adv. Polym. Sci.* **168** 51–246

[12] Niemz M H, Klancnik E G and Bille J F 1991 Plasma-mediated ablation of corneal tissue at 1053 nm using a Nd:YLF oscillator/regenerative amplifier laser *Lasers Surg. Med.* **11** 426–31

[13] Liu X, Du D and Mourou G 1997 Laser ablation and micromachining with ultrashort laser pulses *IEEE J. Quantum Electron.* **33** 1706–16

[14] Hwang D J, Choi T Y and Grigoropoulos C P 2004 Liquid-assisted femtosecond laser drilling of straight and three-dimensional microchannels in glass *Appl. Phys.* A **79** 605–12

[15] Loesel F H, Fischer J P, Götz M H, Horvath C, Juhasz T, Noack F, Suhm N and Bille J F 1998 Non-thermal ablation of neural tissue with femtosecond laser pulses *Appl. Phys.* B **66** 121–8

[16] Kondo T, Yamasaki K, Juodkazis S, Matsuo S, Mizeikis V and Misawa H 2004 Three-dimensional microfabrication by femtosecond pulses in dielectrics *Thin Solid Films* **453–454** 550–6

[17] Wolfe D B, Ashcom J B, Hwang J C, Schaffer C B, Mazur E and Whitesides G M 2003 Customization of poly(dimethylsiloxane) stamps by micromachining using a femtosecond-pulsed laser *Adv. Mater.* **15** 62–5

[18] Li Y, Itoh K, Watanabe W, Yamada K, Kuroda D, Nishii J and Jiang Y Y 2001 Three-dimensional hole drilling of silica glass from the rear surface with femtosecond laser pulses *Opt. Lett.* **26** 1912–4

[19] Kim K H and Guo Z 2004 Ultrafast radiation heat transfer in laser tissue welding and soldering *Numer. Heat Transfer* A **46** 23–46

[20] Guo Z, Wan S K, August D A, Ying J, Dunn S M and Semmlow J L 2006 Optical imaging of breast tumor through temporal log-slope difference mappings *Comput. Biol. Med.* **36** 209–23

[21] Gertzman A A and Schuler M 2007 private communications

[22] Sharobaro V I, Moroz V Y, Starkov Y G and Yudenich A A 2008 Treatment of post-burn scar deformations using tissue expansion and endoscopy *Ann. Burns Fire Disasters* **21** 31–7

[23] Jaunich M, Raje S, Kim K H, Mitra K and Guo Z 2008 Bio-heat transfer analysis during short pulse laser irradiation of tissues *Int. J. Heat Mass Transfer* **51** 5511–21

[24] Chang-Yen D A, Eich R K and Gale B K 2005 A monolithic PDMS waveguide system fabricated using soft-lithography techniques *J. Lightwave Technol.* **23** 2088–93

[25] Baudach S, Bonse J and Kautek W 1999 Ablation experiments on polyimide with femtosecond laser pulses *Appl. Phys.* A **69** S395–8

[26] Rubahn K, Ihlemann J, Jakopic G, Simonsen A C and Rubahn H-G 2004 UV laser-induced grating formation in PDMS thin films *Appl. Phys.* A **79** 1715–9

[27] Rosenfeld A, Lorenz M, Stoian R and Ashkenasi D 1999 Ultrashort laser pulse damage threshold of transparent materials and the role of incubation *Appl. Phys.* A **69** S373–6

[28] MELLES GRIOT 2008 Gaussian Beam Optics, available at www.mellesgriot.com

[29] Yariv A 1989 *Quantum Electronics* 3rd edn (New York: Wiley)

[30] Guo Z, Maruyama S and Komiya A 1999 Rapid yet accurate measurement of mass diffusion coefficients by phase shifting interferometer *J. Phys. D: Appl. Phys.* **32** 995–9